Since January 2020 Elsevier has created a COVID-19 resource centre with free information in English and Mandarin on the novel coronavirus COVID-19. The COVID-19 resource centre is hosted on Elsevier Connect, the company's public news and information website.

Thin Solid Films 692 (2019) 137637

Contents lists available at ScienceDirect

Thin Solid Films

journal homepage: www.elsevier.com/locate/tsf

Correlation between electrical properties and cation distribution in $[(Ni_xMn_{1-x})_{0.84}Cu_{0.16}]_3O_4$ thin films prepared by metal-organic decomposition for microbolometer applications

Yong Ho Choi[a,b], Dahl-Young Khang[b,*], Jeong Ho Cho[a,*]

[a] Electronic Materials & Component Center, Korea Institute of Ceramic Engineering & Technology, Jinju 52851, Korea
[b] Department of Materials Science and Engineering, Yonsei University, Seoul 03722, Korea

ARTICLE INFO

Keywords:
Copper-nickel manganite
Metal-organic decomposition
Microbolometer
Temperature coefficient

ABSTRACT

$[(Ni_xMn_{1-x})_{0.84}Cu_{0.16}]_3O_4$ ($0.20 \leq x \leq 0.40$) thin films have been prepared using the metal-organic decomposition method for microbolometer applications. Spinel thin films with a thickness of approximately 100 nm were obtained from the $[(Ni_xMn_{1-x})_{0.84}Cu_{0.16}]_3O_4$ films annealed at the low temperature of 380 °C for 5 h, which enables their direct integration onto substrates having complementary metal-oxide-semiconductor (CMOS) read-out circuitry. To obtain negative-temperature-coefficient films with reasonable performance through low enough temperature anneal process, Ni content has been systematically varied, and the film microstructure has been found to depend on the relative amount of Ni and Mn. A single phase of cubic spinel structure has been confirmed in the prepared films. The resistivity (ρ) of the annealed films decreases with increasing Mn^{4+}/Mn^{3+} value due to the hopping mechanism between Mn^{3+} and Mn^{4+} cations in octahedral sites of spinel structure. Although the temperature coefficient of resistance (TCR) of the annealed films has been decreased slightly with the increase of Ni content, good enough properties of the film (ρ = 61.3 Ω•cm, TCR = −2.950%/K in $x = 0.30$ film) has been obtained even with the annealing at rather low temperature of 380 °C, thus enabling the direct integration onto substrates having read-out circuitry. The results obtained in this work are promising for applications to CMOS integrated microbolometer devices.

1. Introduction

Since the beginning of the 21st century, there has been growing interest in infra-red (IR) sensors, as IR imaging cameras are a key device to detect and block acute epidemics such as severe acute respiratory syndrome, Influenza A, Ebola, middle east respiratory syndrome, and Zika virus at an early stage.

Compared with cooled detectors, uncooled microbolometers are the most preferred IR imagers due to several significant advantages, such as their low cost, low power consumption, room-temperature operation, compactness, high durability, and light weight [1]. Thus far, various sensing materials for uncooled microbolometers have been studied. Among them, vanadium oxide is the most widely used given its high temperature coefficient of resistance (TCR; >2.5%/K) and low-cost preparation methods [1,2]. However, this material shows a narrow operating temperature window due to the semiconductor-metal transition at ~67 °C, as well as difficulty in controlling the precise composition during deposition [2–4].

Recently, various efforts have been made to find alternative bolometer-sensing materials. Spinel materials based on nickel manganite are one of such promising materials. Until now, nickel manganite based spinel thin films have been fabricated by various methods [5–8]. Kong et al. fabricated Mn-Co-Ni-O (MCN) thin films by RF magnetron sputtering method [5]. Ji et al. also fabricated MCN thin films using laser molecular beam epitaxy technique [6]. However, these vacuum processes have the disadvantage of expensive process costs. Several groups including He et al. fabricated nickel manganite based spinel thin films using chemical solution deposition method, but it requires a relatively high annealing temperature [7,8]. In previous study, we have also fabricated $[(Ni_{0.2}Mn_{0.8})_{1-x}\ Cu_x]_3O_4$ ($0.25 \leq x \leq 0.40$) thin films using the metal-organic decomposition (MOD) method, and demonstrated that the thin films have high absolute TCR values (>3%/K) and low resistivity (<50 Ω cm) [4]. Although the TCR and resistivity outcomes are sufficient, it is not easy to apply them for use in an uncooled microbolometer because the annealing temperature is too high (450 °C). Temperature-sensing materials for a microbolometer require a low

* Corresponding authors.
E-mail addresses: dykhang@yonsei.ac.kr (D.-Y. Khang), goedc@kicet.re.kr (J.H. Cho).

https://doi.org/10.1016/j.tsf.2019.137637
Received 17 May 2019; Received in revised form 4 October 2019; Accepted 13 October 2019
Available online 16 October 2019

annealing temperature (≤400 °C) for the direct integration onto a substrate having complementary metal-oxide-semiconductor (CMOS) read-out circuitry [9].

It is well known that, in spinel manganite materials, cations are localized at tetrahedral (A) and octahedral (B) sites and the electrical conduction is based on the electron hopping between Mn^{3+} and Mn^{4+} in B sites [10]. Resistivity is dependent on the cation distribution, i.e., the ratio of Mn^{3+} and Mn^{4+} in B sites, and the ratio can be changed by controlling the amount of Ni^{2+} in B sites [11]. Thus, the control of nickel and manganese composition has a great influence on the electrical properties of manganite materials and can lower the annealing temperature while maintaining reasonable level of electrical properties.

In this work, the microstructures and electrical properties of $[(Ni_xMn_{1-x})_{0.84}Cu_{0.16}]_3O_4$ thin films prepared by MOD are investigated as a function of the Ni content ($0.20 \le x \le 0.40$). For more stable CMOS compatibility, the process was carried out at a low temperature of 380 °C, and the TCR and resistivity values of the films were characterized.

2. Experiment

The starting materials were MOD coating solutions of NiO (0.5 mol/L), $MnO_{1.5}$ (0.5 mol/L), and CuO (0.4 mol/L) supplied by Kojundo Chemical Laboratory, Japan. The precursor solutions were mixed according to the chemical formula of $[(Ni_xMn_{1-x})_{0.84}Cu_{0.16}]_3O_4$ and were blended with butyl acetate to enhance the coatability onto substrate. The mixed solution was spin-coated at 3000 rpm for 15 min on cleaned SiN_x (200 nm)/Si substrates (1 inch × 1 inch). In order to decompose the precursor materials and prepare an amorphous metal oxide thin film, the deposited film was baked at 200 °C for 30 min. These baked films were further annealed at 380 °C for 5 h in air for crystallization.

The thickness and surface morphology of the annealed films were characterized using a field-emission scanning electron microscope (FE-SEM, JSM-6700F, Jeol, Japan) operating at an accelerating voltage of 10 kV and an atomic force microscope (AFM, A100-AFM, APE Research, Italy). The elemental distribution of Ni, Mn and Cu ions at the surface of the annealed films was investigated by means of X-ray photoelectron spectroscopy (XPS, PHI 5000 Versa Probe™, ULVAC-PHI, Japan) using monochromatized Al Kα (1486.6 eV) X-ray source with a power of 25.3 W. The XPS spectra were obtained with the analyzer pass energy of 23.5 eV and the electron take-off angle was set at 45°. The beam diameter was 100 μm. The binding energies were calibrated based on the C1s peak at 284.8 eV. The resulting spectra were fitted with the Multipak software. Fitting was performed after Shirley background subtraction and XPS peaks were deconvoluted as Gaussian-Lorentzian components with specified binding energy value for each element. The formation of spinel structure was identified using Fourier-transform infra-red (FT-IR, Nicolet iS50, Thermo, USA) spectroscopy. The resistivity of the thin films was measured by the four-point probe system (VP75, DSF System, Korea) in a temperature range of 25 °C to 85 °C.

3. Results and discussion

Cross-sectional FE-SEM images of $[(Ni_xMn_{1-x})_{0.84}Cu_{0.16}]_3O_4$ thin films annealed at 380 °C for 5 h are shown in Fig. 1. The thicknesses of all annealed films, regardless of the Ni content, are very thin (about 100 nm). The annealed films and SiN_x/Si substrates have good adhesion without any delamination. It should be noted that the film surface seems non-flat for rather low Ni content ($x = 0.2 \sim 0.35$), while other samples show quite flat surface for higher Ni incorporation ($x = 0.4$). This difference in surface morphology, depending upon the content of Ni, can be clearly seen in the top-view FE-SEM images of the sample surfaces, as shown in Fig. 2. Protruding net-like morphology was formed on film surfaces for rather low Ni content. As the Ni content increases up to 0.4, however, the net-like undulation disappears completely and the film surface gets flat.

Fig. 3 shows AFM images of film surfaces for different Ni contents ($x = 0.2$ and 0.4), which clearly demonstrates the drastic difference in surface morphology depending upon the Ni content. These results show that Ni plays an important role in improving the surface morphology by removing the net-like structures. Similar flattening effect of Ni addition has been reported: Mn doped ZnO thin film prepared by sol-gel spin coating formed a wave like nematic structure, while Ni doped ZnO thin film was flat [12].

Fig. 4 shows the FT-IR spectra of $[(Ni_xMn_{1-x})_{0.84}Cu_{0.16}]_3O_4$ thin films annealed at 380 °C for 5 h. Three main peaks were detected at 513, 565 and 611 cm^{-1} [13,14], which confirms the formation of a single phase cubic spinel structure in all the samples. 513, 565 and 611 cm^{-1} peaks denote Ni-O bond on B sites, Mn-O bond on B sites and Mn-O(A_{1g}) bond on A sites, respectively [14].

The XPS was used to study the valences and distributions of the Mn, Cu, and Ni ions in the spinel structure. Fig. 5(a) and (b) show the XPS spectra for Mn $2p_{3/2}$ and Cu $2p_{3/2}$ of a $[(Ni_xMn_{1-x})_{0.84}Cu_{0.16}]_3O_4$ ($x = 0.25$) thin film samples, respectively. The Mn $2p_{3/2}$ peak was deconvoluted into three peaks of Mn^{2+}, Mn^{3+} and Mn^{4+} at the corresponding binding energies of 641.0 eV, 642.3 eV and 644.0 eV, respectively [5]; similarly, the Cu $2p_{3/2}$ peak was deconvoluted into two peaks of Cu^+ and Cu^{2+} at binding energies of 930.9 eV and 933.4 eV, respectively [15]. Table 1 shows the percentage of each valence of Mn and Cu calculated from the integration of each deconvoluted peak. Mn^{2+} content increases with increasing Ni content while Mn^{3+} content decreases. The content of Mn^{4+} increases from 8% at $x = 0.20$ to 19% at $x = 0.25$, and remained almost constant up to $x = 0.40$. Cu^{2+} content decreases with increasing Ni content while Cu^+ content varies rather randomly.

Cu^+ mainly occupies A-sites, while Cu^{2+} takes on both A and B sites [16,17]. Ni^{2+}, Mn^{3+} and Mn^{4+} prefer the occupation of B-sites while Mn^{2+} does A-sites [16]. Moreover, the octahedral preferences of Cu^{2+}, Ni^{2+}, Mn^{3+} and Mn^{4+} are in the order of $Mn^{4+} > Mn^{3+} > Ni^{2+} > Cu^{2+}$, while Cu^+ and Mn^{2+} have a high tendency to occupy A-sites [15]. According to these empirical rules, Cu^+ and Mn^{2+} ions fill A-sites preferentially, and Cu^{2+} ion (has lower priority for B-sites) then fills the remaining fraction of A-sites. On the other hand, B-sites are occupied by other cations (Ni^{2+}, Mn^{3+}, Mn^{4+}, and excess Cu^{2+}). To calculate the cation distribution in AB_2O_4 spinel film, the fraction of each cation for A and B sites should be quantified. For a given Ni fraction (experimental variable), the quantity of Ni, Mn, and Cu in $[(Ni_xMn_{1-x})_{0.84}Cu_{0.16}]_3O_4$ film can easily be calculated. For $x = 0.2$ as an example, simple calculation leads to $Ni_{0.504}Mn_{2.016}Cu_{0.480}O_4$, which shows the total amount of Ni, Mn, and Cu. Then, for multi-valence ions of Mn and Cu, the fraction of each valence cation can be calculated by multiplying the relative abundance measured by XPS (given in Table 1). For Mn, the quantity of Mn^{2+} cation is calculated to be 0.872 (=43.23% %× 2.016). The quantity of other cations such as Mn^{3+}, Mn^{4+}, Cu^+, and Cu^{2+} can be obtained by similar procedure. Finally, the spinel film AB_2O_4 should be filled with cations, based on empirical rules discussed above, as [Mn^{2+}, Cu^+, Cu^{2+}] ions for A sites and [Ni^{2+}, Mn^{3+}, Mn^{4+}, Cu^{2+}] ions for B sites, respectively. For the A sites, the sum of three cations should be unity, while that for the B sites be two. Note here that Cu^{2+} ions fill A sites that are not filled with Mn^{2+} and Cu^+. The remaining Cu^{2+} ions then fill the B sites. Table 2 shows the calculated cation distribution in each prepared $[(Ni_xMn_{1-x})_{0.84}Cu_{0.16}]_3O_4$ ($0.20 \le x \le 0.40$) thin films.

It should be noted that, as the Ni content increases, the ratio of Mn^{3+} and Mn^{4+} in the B sites approaches to unity. The conductivity is known to have maximum when the numbers of Mn^{3+} and Mn^{4+} are identical [18]. In other words, the resistivity tends to decrease when the ratio of Mn^{3+} and Mn^{4+} in the B sites approaches unity, which agrees well with our experimentally measured data shown in Fig. 6.

Fig. 7 shows the resistivity of $[(Ni_xMn_{1-x})_{0.84}Cu_{0.16}]_3O_4$ thin films annealed at 380 °C for 5 h, as a function of temperature. As the temperature increases, the resistivity decreases, which is a typical

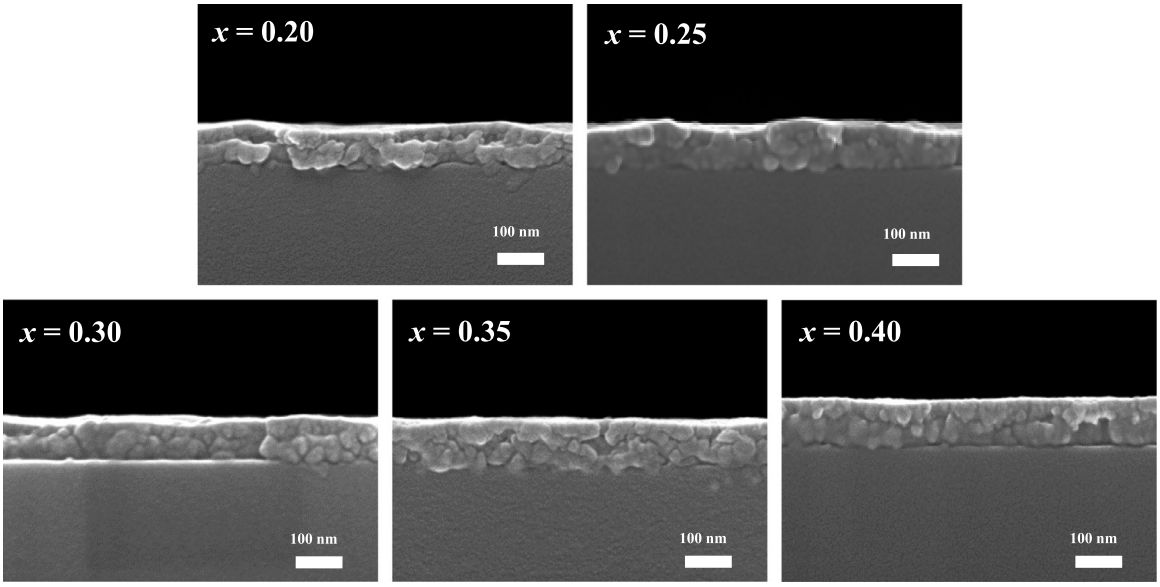

Fig. 1. Cross-sectional FE-SEM images of $[(Ni_xMn_{1-x})_{0.84}Cu_{0.16}]_3O_4$ thin films annealed at 380 °C for 5 h.

characteristics of negative-temperature-coefficient (NTC) thermistor. Further, the resistivity decreases with the increase of Ni content in the films. In order to explain the electrical properties of NTC materials based on nickel-manganite, it is necessary to understand the small polaron hopping model as well as the surface morphology [7]. The electrical conductivity of nickel-manganite-based NTC materials is affected by carrier hopping between Mn^{4+} and Mn^{3+} ions at the B sites [16,19]. Therefore, the dependence of the resistivity on the Mn^{4+}/Mn^{3+} values in Fig. 6 is due to the carrier hopping between Mn^{3+} and Mn^{4+}. As shown in Table 2, Ni plays a role in controlling the ratio of Mn^{3+} and Mn^{4+} in B sites. The small polaron hopping model is expressed by the following equation [20],

$$\rho(T) = CT^{\alpha} \exp(T_0/T)^{p}, \quad (1)$$

where C is a constant, T is the absolute temperature, α and p are power law exponents, and T_0 is the characteristic temperature. When $\alpha = = p = 1$, the electron hopping model becomes the nearest-neighbor hopping (NNH) model, and the spinel manganite film generally follows the NNH model. Therefore, the expression of Eq. (1) can be rewritten as follows:

$$\rho(T) = CT \exp(T_0/T) \quad (2)$$

From the plot of $\ln(\rho/T)$ vs $1/T$ as shown in Fig. 8, the linear regression analysis yields T_0, which is proportional to E_a in the NNH model. E_a can be calculated from the following equation [8],

$$E_a = T_0 k_B, \quad (3)$$

where k_B is the Boltzmann constant. The values of calculated T_0 and E_a are listed in Table 3.

It was suggested by Elbadraoui et al. that electron conduction may also proceed via jumping between Mn^{3+} and Mn^{4+} ions on more distant B-sites through Cu^{+} and Cu^{2+} ions at the A-sites [10]. This process can be expressed as follows: $Mn_B^{3+} + Cu_A^{2+} + Mn_B^{4+} \leftrightarrow Mn_B^{4+} + Cu_A^{+} + Mn_B^{4+} \leftrightarrow Mn_B^{4+} + Cu_A^{2+} + Mn_B^{3+}$ [16]. Considering the fact that the Cu content does not show any meaningful trend as shown in Table 1, however, we believe that this mechanism would not have a strong influence on changes in the electrical characteristics.

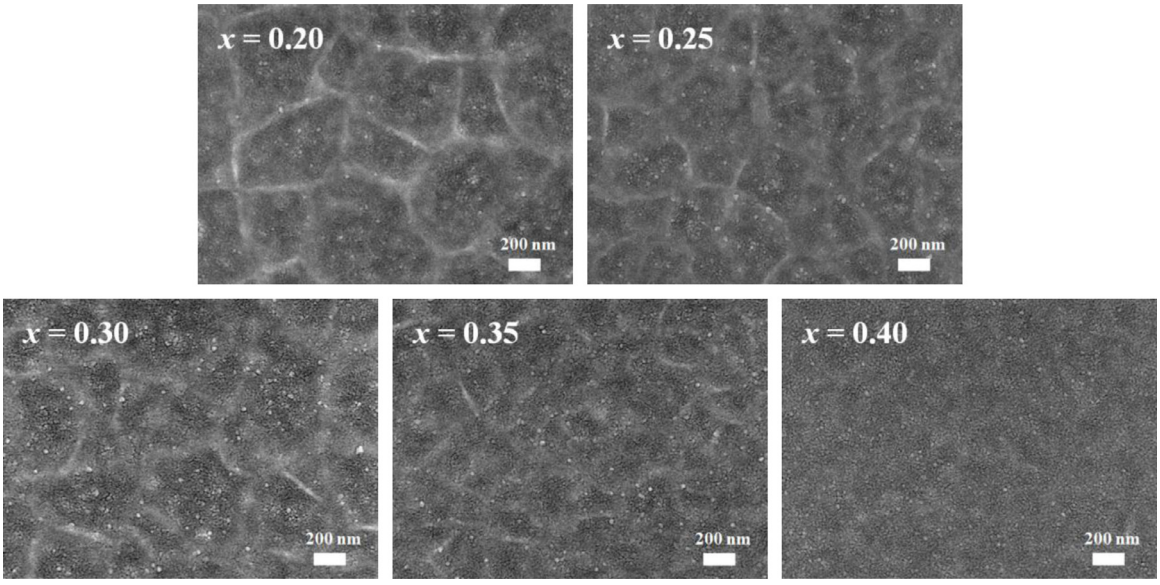

Fig. 2. Top-view FE-SEM images of $[(Ni_xMn_{1-x})_{0.84}Cu_{0.16}]_3O_4$ thin films as a function of Ni content.

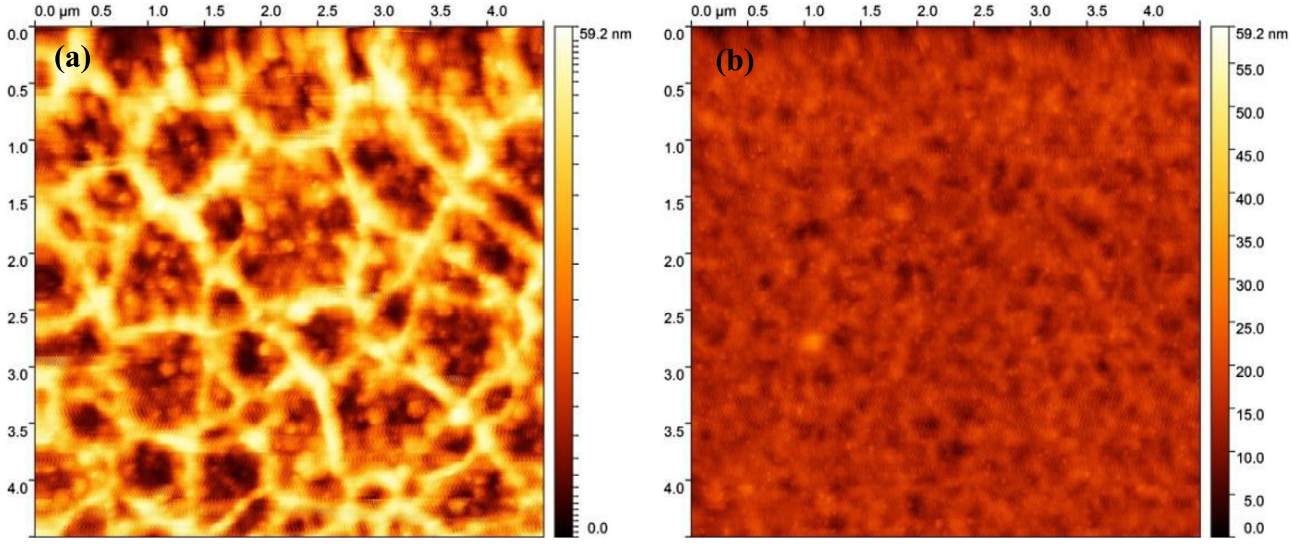

Fig. 3. AFM images of $[(Ni_xMn_{1-x})_{0.84}Cu_{0.16}]_3O_4$ thin films for (a) $x = 0.2$, and (b) $x = 0.4$, respectively (z-scale is 59.2 nm for both images).

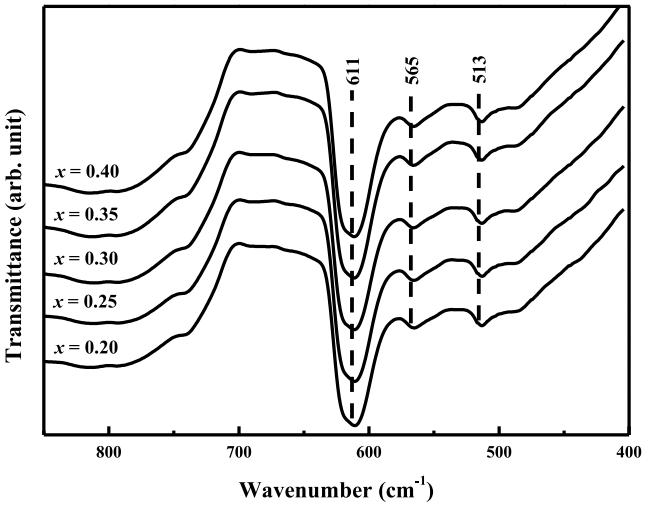

Fig. 4. FT-IR spectra of $[(Ni_xMn_{1-x})_{0.84}Cu_{0.16}]_3O_4$ thin films.

An important factor with regard to the sensitivity of NTC films is the TCR value. The TCR value at 298 K (T) can be evaluated using the following equation [8]:

Table 1.
Ions valences and their abundance in $[(Ni_xMn_{1-x})_{0.84}Cu_{0.16}]_3O_4$ thin films by XPS.

x (mol)	Mn^{3+}(%)	Mn^{4+}(%)	Mn^{2+}(%)	Cu^{+}(%)	Cu^{2+}(%)
0.20	43	49	8	4	96
0.25	44	37	19	6	94
0.30	49	32	19	5	95
0.35	55	25	20	5	95
0.40	56	25	19	7	93

$$TCR(\%/K) = -100T_0/T^2 \quad (4)$$

Table 3 shows that the TCR of the annealed films decreased with an increase of Ni content (x) in the film, which shows the same trend to the change in T_0 and E_a.

4. Conclusions

Single-phase cubic spinel structure $[(Ni_{0.2}Mn_{0.8})_{1-x}Cu_x]_3O_4$ ($0.20 \le x \le 0.40$) thin films were fabricated by metal-organic decomposition. The annealed films (~ 100 nm thick) showed NTC thermistor characteristics with a decrease in the resistivity upon an increase in the temperature. The morphological uniformity has been improved with the increase of Ni content, while the electrical resistivity was decreased

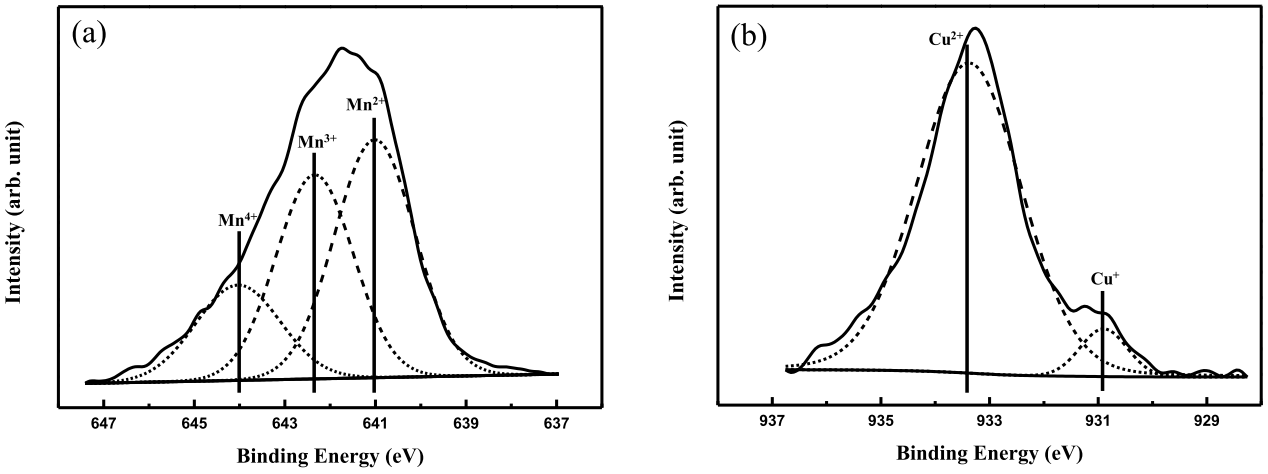

Fig. 5. XPS spectra (Mn $2p_{3/2}$ and Cu $2p_{3/2}$) of $[(Ni_xMn_{1-x})_{0.84}Cu_{0.16}]_3O_4$ thin film for $x = 0.25$.

Table 2.
Cation distribution in $[(Ni_xMn_{1-x})_{0.84}Cu_{0.16}]_3O_4$ thin films.

x (mol)	Cation distribution	Mn^{4+}/Mn^{3+}
0.20	$[Mn_{0.87}^{2+}\ Cu_{0.02}^{+}Cu_{0.11}^{2+}]_A[Ni_{0.50}^{2+}Mn_{0.99}^{3+}Mn_{0.16}^{4+}Cu_{0.35}^{2+}]_BO_4^{2-}$	0.16
0.25	$[Mn_{0.84}^{2+}\ Cu_{0.03}^{+}Cu_{0.13}^{2+}]_A[Ni_{0.63}^{2+}Mn_{0.69}^{3+}Mn_{0.36}^{4+}Cu_{0.32}^{2+}]_BO_4^{2-}$	0.52
0.30	$[Mn_{0.88}^{2+}\ Cu_{0.02}^{+}Cu_{0.10}^{2+}]_A[Ni_{0.76}^{2+}Mn_{0.56}^{3+}Mn_{0.33}^{4+}Cu_{0.35}^{2+}]_BO_4^{2-}$	0.59
0.35	$[Mn_{0.90}^{2+}\ Cu_{0.02}^{+}Cu_{0.08}^{2+}]_A[Ni_{0.88}^{2+}Mn_{0.42}^{3+}Mn_{0.32}^{4+}Cu_{0.38}^{2+}]_BO_4^{2-}$	0.76
0.40	$[Mn_{0.86}^{2+}\ Cu_{0.03}^{+}Cu_{0.11}^{2+}]_A[Ni_{1.01}^{2+}Mn_{0.37}^{3+}Mn_{0.29}^{4+}Cu_{0.33}^{2+}]_BO_4^{2-}$	0.78

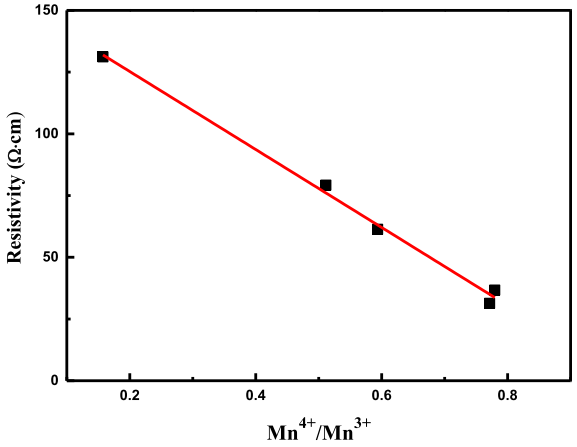

Fig. 6. Dependence of resistivity at room temperature on the ratio of Mn^{4+}/Mn^{3+} in $[(Ni_xMn_{1-x})_{0.84}Cu_{0.16}]_3O_4$ thin films.

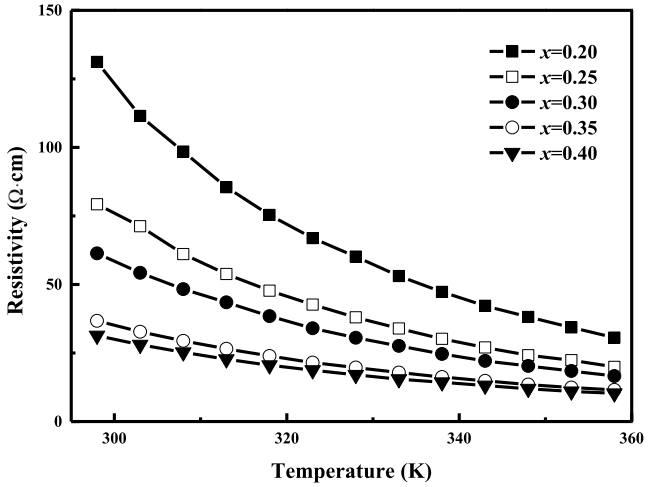

Fig. 7. Resistivity of $[(Ni_xMn_{1-x})_{0.84}Cu_{0.16}]_3O_4$ thin films as a function of temperature.

from 131.2 Ω cm to 31.3 Ω cm. Concurrently, the increase of Ni content has also led to the increase in the ratio of Mn^{4+}/Mn^{3+} close to unity, leading to the decrease in resistivity. This is because the Mn ions at the B sites have strong contribution to the electrical properties of the films by participating in hopping transport. Although the T_0 (from 2876 K to 2314 K), E_a (from 0.2479 eV to 0.1995 eV), and TCR (from −3.196%/K to −2.571%/K) decrease slightly with the increase of Ni content x (from 0.20 to 0.40), the processing temperature could be reduced below 400°C, which enables the direct integration of the materials onto substrates having CMOS read-out circuitry. The demonstrated Ni-Mn-Cu-O thin films prepared at low enough temperature (380 °C) has shown good enough performance (ρ = =61.3 Ω cm, TCR = − =2.950%/K in x = =0.30 film) as NTC materials for microbolometer applications.

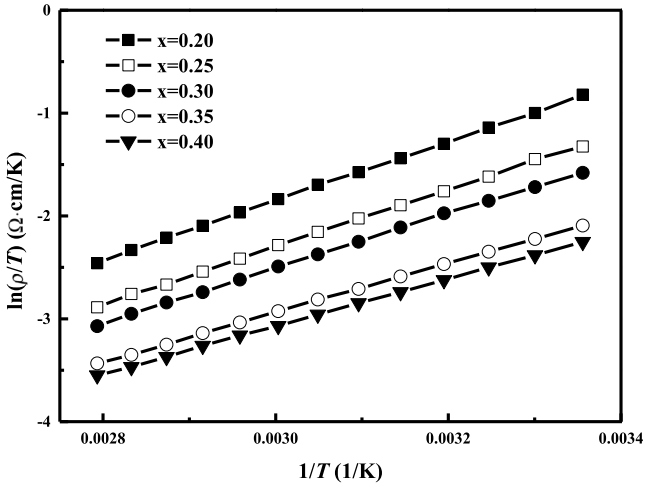

Fig. 8. Plots of ln(ρ/T) versus 1/T for $[(Ni_xMn_{1-x})_{0.84}Cu_{0.16}]_3O_4$ thin films.

Table 3.
The characteristic temperature (T_0), activation energy (E_a) and temperature coefficient of resistance (TCR) of $[(Ni_xMn_{1-x})_{0.84}Cu_{0.16}]_3O_4$ thin films.

x (mol)	T_0 (K)	E_a (eV)	TCR (%/K)
0.20	2876	0.2479	−3.196
0.25	2794	0.2408	−3.104
0.30	2655	0.2289	−2.950
0.35	2398	0.2067	−2.664
0.40	2314	0.1995	−2.571

Declaration of Competing Interest

The authors declare that they have no known competing financial interests or personal relationships that could have appeared to influence the work reported in this paper.

The authors declare the following financial interests/personal relationships which may be considered as potential competing interests:

Acknowledgements

This work was supported by a grant from the Fundamental R&D program funded by the Korea Institute of Ceramic Engineering and Technology (KICET) and Ministry of Trade, Industry and Energy (MOTIE), Republic of Korea. This work was also supported by Basic Science Research Program through the National Research Foundation of Korea (NRF) funded by the Ministry of Education (NRF-2019R1A6A1A11055660).

References

[1] E. Battal, S. Bolat, M.Y. Tanrikulu, A.K. Okyay, T. Akin, Atomic-layer-deposited zinc oxide as tunable uncooled infrared microbolometer material, Phys. Status Solidi A 211 (2014) 2475–2482.
[2] H.Y. Lee, C.L. Wu, C.H. Kao, C.T. Lee, S.F. Tang, W.J. Lin, H.C. Chen, J.C. Lin, Investigated performance of uncooled tantalum-doped VO_x floating-type microbolometers, Appl. Surf. Sci. 354 (2015) 106–109.

[3] C. Ouyang, W. Zhou, J. Wu, Y. Hou, Y. Gao, Z. Huang, Uncooled bolometer based on Mn1.56Co0.96Ni0.48O4 thin films for infrared detection and thermal imaging, Appl. Phys. Lett. 105 (2014) 022105.
[4] C.J. Jeon, Y.H. Jeong, J.S. Yun, W.I. Park, J.H. Paik, Y.W. Hong, E.S. Kim, J.H. Cho, Electrical properties of copper-nickel manganite thin films prepared by metal-organic decomposition, Ceram. Int. 43 (2017) 9291–9295.
[5] W. Kong, W. Wei, B. Gao, A. Chang, A study on the electrical properties of Mn-Co-Ni-O thin films grown by radio frequency magnetron sputtering with different thicknesses, Appl. Surf. Sci. 423 (2017) 1012–1018.
[6] G. Ji, A. Chang, J. Xu, H. Zhang, J. Hou, B. Zhang, P. Zhao, Low-temperature (< 300 °C) growth and characterization of single-[100]-oriented Mn-Co-Ni-O thin films, Mater. Lett. 107 (2013) 103–106.
[7] L. He, G. Zhang, Z.Y. Ling, Improvement of structural and electrical properties of Mn-based thin film thermistors by a bilayer structure, Mater. Lett. 128 (2014) 144–147.
[8] Y.Q. Gao, Z.M. Huang, Y. Hou, J. Wu, W. Zhou, C. Ouyang, J.G. Huang, J.C. Tong, J.H. Chu, Structural and electrical properties of $Mn_{1.56}Co_{0.96}Ni_{0.48}O_4$ NTC thermistor films, Mater. Sci. Eng. B 185 (2014) 74–78.
[9] S.W. Ko, J. Li, N.J. Podraza, E.C. Dickey, S. Trolier-McKinstry, Spin spray-deposited nickel manganite thermistor films for microbolometer applications, J. Am. Ceram. Soc. 94 (2011) 516–523.
[10] C. Zhao, B. Wang, P. Yang, L. Winnubst, C. Chen, Effects of Cu and Zn co-doping on the electrical properties of $Ni_{0.5}Mn_{2.5}O_4$ NTC ceramics, J. Eur. Ceram. Soc. 28 (2008) 35–40.
[11] A. Feteiar, Negative temperature coefficient resistance (NTCR) ceramic thermistors: an industrial perspective, J. Am. Ceram. Soc. 92 (2009) 967–983.
[12] G. Vijayaprasath, R. Murugan, G. Ravi, T. Mahalingam, Y. Hayakawa, Characterization of dilute magnetic semiconducting transition metal doped ZnO thin films by sol–gel spin coating method, Appl. Surf. Sci. 313 (2014) 870–876.
[13] R.N. Jadhav, V. Puri, Microwave absorption, conductivity and complex pemittivity of fritless $Ni_{(1-x)}Cu_xMn_2O_4$ ($0 \leq x \leq 1$) ceramic thick film: effect of copper, Prog. Electromagn. Res. 8 (2009) 149–160.
[14] N.M. Hagh, G.G. Amatucci, A new solid-state process for synthesis of $LiMn_{1.5}Ni_{0.5}O_{4-\delta}$ spinel, J. Power Sources 195 (2010) 5005–5012.
[15] C. Drouet, C. Laberty, J.L.G. Fierro, P. Alphonse, A. Rousset, X-ray photoelectron spectroscopic study of non-stoichiometric nickel and nickel–copper spinel manganites, Int. J. Inorg. Mater. 2 (2000) 419–426.
[16] E. Elbadraoui, J.L. Baudour, F. Bouree, B. Gillot, S. Fritsch, A. Rousset, Cation distribution and mechanism of electrical conduction in nickel-copper manganite spinels, Solid State Ionics 93 (1997) 219–225.
[17] O.S. Aleksic, M.V. Nikolic, M.D. Lukovic, N. Nikolic, B.M. Radojcic, M. Radovanovic, Z. Djuric, M. Mitric, P.M. Nikolic, Preparation and characterization of Cu and Zn modified nickel manganite NTC powders and thick film thermistors, Mater. Sci. Eng. B 178 (2013) 202–210.
[18] K. Park, Fabrication and electrical properties of Mn-Ni-Co-Cu-Si oxides negative temperature coefficient thermistors, J. Am. Ceram. Soc. 88 (2005) 862–866.
[19] H.J. Jeong, J.M. Cha, B.K. Ryu, Study on the electrical conductivity and catalytic property by structural change of $70V_2O_5$-$10Fe_2O_3$-$13P_2O_5$-$7B_2O_3$ glass with crystallization, J. Korean Ceram. Soc. 54 (2017) 406–412.
[20] R. Schmidt, A. Basu, A.W. Brinkman, Z. Klusek, P.K. Datta, Electron-hopping modes in $NiMn_2O_{4+\delta}$ materials, Appl. Phys. Lett. 86 (2005) 073501.